JOINT SCALAR VS. JOINT VELOCITY-SCALAR PDF MODELLING OF BLUFF-BODY STABILISED FLAMES WITH REDIM

Bart Merci
Postdoctoral Fellow of the Fund of Scientific Research - Flanders (Belgium) (FWO-Vlaanderen)
Ghent University - UGent, Dept. of Flow, Heat and Combustion Mechanics
Bart.Merci@UGent.be

Bertrand Naud
Modeling and Numerical Simulation Group, Energy Department
Ciemat, Madrid, Spain
Bertrand.Naud@ciemat.es

Dirk Roekaerts
Delft University of Technology, Department of Multi-Scale Physics
Delft, The Netherlands
d.j.e.m.roekaerts@tudelft.nl

Ulrich Maas
Karlsruhe University (TH), Institute for Technical Thermodynamics
Karlsruhe, Germany
umaas@itt.uni-karlsruhe.de

ABSTRACT

Two transported PDF strategies (joint velocity-scalar and joint scalar PDF) are investigated for bluff-body stabilised turbulent diffusion flames with variable degree of turbulence - chemistry interaction. Chemistry is modeled by the novel REDIM technique. The (second-moment closure) turbulence model and the (modified Curl's) micro-mixing model are not varied. Radiative heat loss effects are ignored. The results for mean velocity and turbulent stresses are very similar for both methods. They agree well with experimental data. Each of the two PDF approaches implies a different closure for the velocity-scalar correlation. This leads to differences in the radial profiles in physical space of mean scalars and mixture fraction variance (due to different scalar flux modelling). Differences are visible in mean mixture fraction and mean temperature, as well as in mixture fraction variance. In general, the joint scalar PDF results are in somewhat better agreement with experimental data. In composition space, where results are reported as scatter plots, differences between the two PDF strategies are small in the calculations at hand, with a little more local extinction in the joint scalar PDF results.

INTRODUCTION

Non-linear interaction between turbulent fluctuations and finite-rate chemistry is important in nonpremixed turbulent flames and may lead to local extinction or incomplete combustion. Turbulence-chemistry interaction modelling is therefore a central issue in non-premixed turbulent flame simulations. Modelling at the level of the joint scalar probability density function (PDF) offers an exact treatment of the chemical reaction source term with a given chemistry model.

In transported PDF methods, based on stochastic Lagrangian modelling as described by Pope (1985), we solve a modelled transport equation for the mass density function (MDF) by a particle stochastic method. The three main modelling ingredients are: turbulence model, chemistry model and micro-mixing model. These sub-models have been the subject of several recent comparative studies. Ren (2004) compared three widely used mixing models in stochastic simulations of partially stirred reactors (PaSR). In the context of transported scalar PDF modelling, the same mixing models are compared by Merci et al. (2006a) for the piloted jet diffusion flame Delft flame III, and by Merci et al. (2006b) for the bluff-body stabilised flames HM1-3. Cao and Pope (2005) compared seven chemical mechanisms for methane/air combustion in joint velocity-scalar-turbulence frequency PDF calculations of the non-premixed piloted jet Sandia flames D, E, and F.

In the present study, the REDIM approach is followed for reduced chemistry modelling (Bykov and Maas, in press). To the best of the authors' knowledge, this is the first application of REDIM to a turbulent non-premixed flame.

Additionally, however, the choice of the PDF description itself has direct consequences on the modelling of the scalar flux (and higher order velocity-scalar correlation). With the joint scalar MDF $\mathcal{F}_\phi$, the gradient diffusion assumption to close the conditional fluctuating velocity term in the MDF transport equation, Eq. (4), leads to a simple algebraic model for the scalar flux. When velocity is included in the PDF description, the transport equation for the joint velocity-scalar MDF $\mathcal{F}_{U\phi}$, Eq. (5), is modelled and solved using a particle method. In this case, the combination of the model a_i for particle velocity evolution and the mixing model θ_α implies a modelled transport equation for the scalar flux (and higher order velocity-scalar correlation).

In the present study, we compare results of joint scalar PDF (JSPDF) and joint velocity-scalar PDF (JVSPDF) simulations, using hybrid Finite-Volume / particle methods implemented in the same in-house computer program 'PDFD' as described by Naud et al. (2006). The same turbulence, chemistry and micro-mixing models are used in all simulations. The flames considered are the Sydney bluff-body stabilised flames HM1 and HM3 (Dally and Masri, 1998; Dally et al., 1998; http://www.aeromech.usyd.edu.au/thermofluids/main_frame.htm). These are target flames of the International Workshop on Measurement and Computation of Turbulent Nonpremixed Flames (http://www.ca.sandia.gov/TNF).

PDF APPROACH

Statistical description

The statistical description of the flow is made in terms of the joint one-point PDF f_Φ such that $f_\Phi(\boldsymbol{\Psi};\boldsymbol{x},t)\,.\mathrm{d}\boldsymbol{\Psi}$ is the probability that $\boldsymbol{\Phi}$ is in the interval $[\boldsymbol{\Psi},\boldsymbol{\Psi}+\mathrm{d}\boldsymbol{\Psi}[$ at point $(\boldsymbol{x},t)$. When JSPDF is consid-

ered, $\boldsymbol{\Phi}$ is the composition vector $\boldsymbol{\phi}$. For JVSPDF, $\boldsymbol{\Phi} = (\boldsymbol{U}, \boldsymbol{\phi})$, with $\boldsymbol{U}$ the velocity vector. The joint PDF is defined as described by Pope (1985,2000):

$$f_{\Phi}(\boldsymbol{\Psi}; \boldsymbol{x}, t) = \langle \delta[\boldsymbol{\Phi}(\boldsymbol{x}, t) - \boldsymbol{\Psi}] \rangle, \tag{1}$$

where $\delta[\,]$ is the Dirac delta function and where the brackets $\langle\,\rangle$ refer to the expected value. Using the conditional expected value, $\langle\, Q(\boldsymbol{x}, t) | \, \boldsymbol{\Psi} \rangle f_{\Phi}(\boldsymbol{\Psi}; \boldsymbol{x}, t) = \langle Q(\boldsymbol{x}, t) \, . \delta[\boldsymbol{\Phi}(\boldsymbol{x}, t) - \boldsymbol{\Psi}] \rangle$, mean values (or expected values) are defined as:

$$\langle Q(\boldsymbol{x}, t) \rangle = \int_{[\boldsymbol{\Psi}]} \langle\, Q(\boldsymbol{x}, t) | \, \boldsymbol{\Psi} \rangle f_{\Phi}(\boldsymbol{\Psi}; \boldsymbol{x}, t) \, . \mathrm{d}\boldsymbol{\Psi}. \tag{2}$$

Fluctuations are defined as: $q'(\boldsymbol{x}, t) = Q(\boldsymbol{x}, t) - \langle Q(\boldsymbol{x}, t) \rangle$.

For variable density flows, it is useful to consider the joint MDF $\mathcal{F}_{\Phi}(\boldsymbol{\Psi}) = \rho(\boldsymbol{\Psi})\, f_{\Phi}(\boldsymbol{\Psi})$. Density weighted (Favre) averages are:

$$\begin{aligned} \widetilde{Q}(\boldsymbol{x}, t) &= \frac{\langle \rho(\boldsymbol{x}, t)\, Q(\boldsymbol{x}, t) \rangle}{\langle \rho(\boldsymbol{x}, t) \rangle} \\ &= \frac{\int_{[\boldsymbol{\Psi}]} \langle\, Q(\boldsymbol{x}, t) | \, \boldsymbol{\Psi} \rangle \mathcal{F}_{\Phi}(\boldsymbol{\Psi}; \boldsymbol{x}, t) \, . \mathrm{d}\boldsymbol{\Psi}}{\int_{[\boldsymbol{\Psi}]} \mathcal{F}_{\Phi}(\boldsymbol{\Psi}; \boldsymbol{x}, t) \, . \mathrm{d}\boldsymbol{\Psi}}. \end{aligned} \tag{3}$$

Fluctuations with respect to the Favre average are defined as: $q''(\boldsymbol{x}, t) = Q(\boldsymbol{x}, t) - \widetilde{Q}(\boldsymbol{x}, t)$.

Scalar PDF transport equation

When the joint scalar MDF $\mathcal{F}_{\phi}$ is considered, the following transport equation is modelled and solved (Pope, 1985):

$$\begin{aligned} &\frac{\partial \mathcal{F}_{\phi}}{\partial t} + \frac{\partial \widetilde{U}_j \mathcal{F}_{\phi}}{\partial x_j} + \frac{\partial}{\partial \psi_{\alpha}} \left[S_{\alpha}(\boldsymbol{\psi})\, \mathcal{F}_{\phi} \right] \\ &= \underbrace{- \frac{\partial}{\partial x_i} \left[\langle\, u_i'' | \, \boldsymbol{\psi} \rangle \mathcal{F}_{\phi} \right]}_{\text{gradient diffusion}} \underbrace{- \frac{\partial}{\partial \psi_{\alpha}} \left[\frac{1}{\rho(\boldsymbol{\psi})} \left\langle - \frac{\partial J_j^{\alpha}}{\partial x_j} \middle| \boldsymbol{\psi} \right\rangle \mathcal{F}_{\phi} \right]}_{\text{mixing model: } \theta_{\alpha}}, \end{aligned} \tag{4}$$

with S_{α} the reaction source term for scalar ϕ_{α} and $\boldsymbol{J}^{\alpha}$ its molecular flux.

Velocity-scalar PDF transport equation

When velocity is included in the PDF description, the transport equation for the joint velocity-scalar MDF $\mathcal{F}_{U\phi}$ can be written (neglecting the mean viscous stress tensor gradient $\partial \langle \tau_{ij} \rangle / \partial x_j$):

$$\begin{aligned} &\frac{\partial \mathcal{F}_{U\phi}}{\partial t} + V_j \frac{\partial \mathcal{F}_{U\phi}}{\partial x_j} \\ &\quad + \left(- \frac{1}{\langle \rho \rangle} \frac{\partial \langle p \rangle}{\partial x_i} + g_i \right) \frac{\partial \mathcal{F}_{U\phi}}{\partial V_i} + \frac{\partial}{\partial \psi_{\alpha}} \left[S_{\alpha}(\boldsymbol{\psi})\, \mathcal{F}_{U\phi} \right] \\ &\quad = - \frac{\partial}{\partial V_i} [a_i \mathcal{F}_{U\phi}] \underbrace{- \frac{\partial}{\partial \psi_{\alpha}} \left[\frac{1}{\rho(\boldsymbol{\psi})} \left\langle - \frac{\partial J_j^{\alpha}}{\partial x_j} \middle| \boldsymbol{V}, \boldsymbol{\psi} \right\rangle \mathcal{F}_{U\phi} \right]}_{\text{mixing model: } \theta_{\alpha}}. \end{aligned} \tag{5}$$

The term a_i denotes:

$$a_i = \left(\frac{1}{\langle \rho \rangle} - \frac{1}{\rho(\boldsymbol{\psi})} \right) \frac{\partial \langle p \rangle}{\partial x_i} + \frac{1}{\rho(\boldsymbol{\psi})} \left\langle - \frac{\partial p'}{\partial x_i} + \frac{\partial \tau_{ij}'}{\partial x_j} \middle| \boldsymbol{V}, \boldsymbol{\psi} \right\rangle \tag{6}$$

The Langevin model for a_i is described in the section on turbulence modelling. The terms on the left hand side of Eq. (5) appear in closed form. Compared to Eq. (4), effects of convection and mean pressure gradient are now exactly accounted for.

HYBRID FINITE-VOLUME / PARTICLE METHOD

Equations (4) and (5) are solved using the consistent hybrid Finite-Volume / particle method as presented by Naud et al. (2006). Mean velocity $\widetilde{\boldsymbol{U}}$, mean pressure gradient $\boldsymbol{\nabla} \langle p \rangle$, Reynolds stresses $\widetilde{u_i'' u_j''}$ and turbulent dissipation rate ϵ are determined using a standard Finite-Volume (FV) method, based on a pressure-correction algorithm.

A set of uniformly distributed computational particles evolves according to the reported stochastic differential equations. Each particle has a set of properties $\{w^*, m^*, \boldsymbol{X}^*, \boldsymbol{\phi}^*\}$ (scalar MDF), or $\{w^*, m^*, \boldsymbol{X}^*, \boldsymbol{u}^*, \boldsymbol{\phi}^*\}$ (velocity-scalar MDF), where w^* is a numerical weight, m^* is the mass of the particle, $\boldsymbol{X}^*$ its position, $\boldsymbol{u}^*$ its fluctuating velocity and $\boldsymbol{\phi}^*$ the particle's composition. The superscript $*$ denotes that the quantity is a stochastic particle property. Particle mass m^* is constant in time. The particle joint scalar MDF is:

$$\mathcal{F}_{\phi}^{P}(\boldsymbol{x}, \boldsymbol{\psi}; t) = \left\langle \sum_{*} w^* m^* . \delta(\boldsymbol{X}^*(t) - \boldsymbol{x}) \, . \delta(\boldsymbol{\phi}^*(t) - \boldsymbol{\psi}) \right\rangle. \tag{7}$$

Additional properties can be deduced for each stochastic particle from the primary properties listed above. As an example, the particle density is obtained as: $\rho^*(t) = \rho[\boldsymbol{\phi}^*(t)]$. Increments of particle position $\boldsymbol{X}^*$ and composition $\boldsymbol{\phi}^*$ over a small time step dt are given by:

$$dX_i^* = (U_i^* + [U_i^c]^*)\, dt, \tag{8}$$

$$d\phi_{\alpha}^* = \theta_{\alpha}^* dt + S_{\alpha}(\boldsymbol{\phi}^*)\, dt. \tag{9}$$

The correction velocity $\boldsymbol{U}^c$ results from a position correction algorithm (Muradoglu et al., 2001), ensuring that the volume represented by the particles in a computational cell, equals the cell geometric volume. With the scalar MDF, $\boldsymbol{U}^*$ results from a random walk model:

$$U_i^* dt = \left[\widetilde{U}_i + \frac{1}{\langle \rho \rangle} \frac{\partial \Gamma_T}{\partial x_i} \right]^* dt + \left[\left(\frac{2 \Gamma_T}{\langle \rho \rangle} \right)^{1/2} \right]^* . dW_i^*, \tag{10}$$

where dW_i^* is an increment over dt of the Wiener process W_i^* and where Γ_T is the turbulent diffusivity, modelled as $\Gamma_T = \mu_T / \mathrm{Sc}_T$, with μ_T the eddy viscosity and the turbulent Schmidt number taken as $\mathrm{Sc}_T = 0.7$. With the joint velocity-scalar MDF, the equations are:

$$U_i^* = \left[\widetilde{U}_i \right]^* + u_i^*, \tag{11}$$

$$du_i^* = - u_j^* \left[\frac{\partial \widetilde{U}_i}{\partial x_j} \right]^* dt + \left[\frac{1}{\langle \rho \rangle} \frac{\partial \langle \rho \rangle \widetilde{u_i'' u_j''}}{\partial x_j} \right]^* dt + a_i^* dt. \tag{12}$$

In the above equations, the quantities between brackets $[\ ]^*$ are FV properties interpolated at the particle location using the bilinear basis functions presented by Jenny et al. (2001). The model for a_i^* is specified below in the section on the turbulence model.

The method of fractional steps, described by Pope (1985), is used to integrate the above systems of equations. In order to ensure second-order accuracy, the 'midpoint rule' is used (Muradoglu et al., 2001; Jenny et al., 2001). A local time-stepping algorithm developed in the framework of statistically stationary problems is applied (Muradoglu and Pope, 2002).

Consistency and coupling

The turbulent dissipation rate is not included in the PDF representation. The transport equation solved for ϵ in the FV method provides additional information, required to model the unclosed terms a_i and θ_{α}. The other FV equations are consistent with the modelled MDF transport equation (Naud et al., 2006).

The mean density $\langle \rho \rangle$ in the FV method is directly obtained from the iteration averaged mean density in the particle method (applying the iteration averaging procedure as presented by Naud et al. (2006)). We remark that the global convergence of the method is improved in comparison to the latter reference, where density relaxation was used.

An outer iteration consists of a number of FV iterations and particle time steps. We use a fixed number of particle time steps (typically 5), while the FV method is iterated until the residuals of all equations start decreasing and the global mean pressure correction is below a specified threshold (with a maximum of 1000 FV iterations per outer iteration).

MODELLING

Turbulence model

A second-moment closure RANS model is applied. From the comparative study presented by Li et al. (2003), the LRR-IPM isotropisation of production model by Launder et al. (1975) is used with the modified constant value $C_{\epsilon 1} = 1.6$, instead of the standard value $C_{\epsilon 1} = 1.44$. Consistently, the Lagrangian isotropisation of production model (LIPM) is used in the velocity-scalar PDF approach to describe velocity evolution a_i (Pope, 1994; Wouters at al., 1996).

Reduced Chemical Model: REDIM

As mentioned, with the transported PDF approach, the chemical reaction source terms are treated exactly. In order to reduce computing times, however, reduced chemistry modelling is applied. The reduced mechanism for the CH_4/H_2/air system is based on a detailed reaction mechanism developed by Chevalier and Warnatz (personal communication), consisting of 34 species and 302 reactions. The concept of reaction/diffusion manifolds (REDIM) (Bykov and Maas, in press) has been used to reduce the system to mixture fraction and one reaction progress variable.

The REDIM concept is based on a relaxation process, where an initial guess for a low-dimensional manifold evolves in such a manner that an invariant slow reaction/diffusion manifold is obtained. The evolution equation for the parametric manifold representation, is:

$$\frac{\partial \Psi_c(\theta)}{\partial t} = \left(I - \Psi_{c,\theta}(\theta)\,\Psi^{+}_{c,\theta}(\theta)\right)\cdot \left(F(\Psi_c) - \frac{1}{\rho} D\Psi_{c,\theta\theta} \circ \mathrm{grad}(\theta) \circ \mathrm{grad}(\theta)\right), \qquad (13)$$

where θ denotes the m-dimensional vector of reduced coordinates, corresponding to the composition vector Ψ_c. In the present model, m=2 and the coordinates are the mass fractions of N_2 and CO_2. Furthermore, t denotes time and D is the diffusion coefficient. Note that equal diffusivities and unity Lewis number have been assumed. The state vector Ψ_c is the $(n = n_s + 2)$-dimensional vector $\Psi_c = \left(h, p, \frac{Y_1}{W_1}, ..., \frac{Y_{n_s}}{W_{n_s}}\right)^T$, where h denotes specific enthalpy, p is pressure, $Y_1, ..., Y_{n_s}$ the n_s species mass fractions and $W_1, ..., W_{n_s}$ the molar masses. $F(\Psi)$ is the n-dimensional thermo-chemical source term vector, $\Psi_{c,\theta}$ the matrix of partial derivatives of the thermokinetic state with respect to the parameterizing variables and $\Psi^{+}_{c,\theta}$ its Moore-Penrose pseudo-inverse. The term $\Psi_{c,\theta\theta} \circ \mathrm{grad}(\theta) \circ \mathrm{grad}(\theta)$ is:

$$\left(\Psi_{c,\theta\theta} \circ \mathrm{grad}(\theta) \circ \mathrm{grad}(\theta)\right)_i = \sum_{j=1}^{m}\sum_{k=1}^{m} \frac{\partial^2 \psi_{c,i}}{\partial\theta_j \partial\theta_k} \mathrm{grad}(\theta_j)\,\mathrm{grad}(\theta_k). \qquad (14)$$

According to Bykov and Maas (in press) the gradients are estimated. In this work we use gradients obtained from typical one-dimensional counterflow diffusion flame calculations:

$$\mathrm{grad}(\theta) = \theta_{\psi_c}\,\mathrm{grad}\psi_c. \qquad (15)$$

It is shown by Bykov and Maas (in press) that the results do not depend very crucially on this assumption.

The initial guess for the evolution equation is a manifold obtained via an interpolation of flamelet solutions, the pure mixing line, and the curve of complete reaction to CO_2 and H_2O. A fine mesh has been chosen in order to resolve the steep gradients. The relaxation to the reaction/diffusion manifold is then performed via a semi-implicit relaxation method. Fig. 1 shows as an example the reaction rates on the manifold for the specific mole numbers of CO_2. The REDIM is then mapped onto a rectangular domain and reaction increments are determined via a pre-integration of the table.

Mixture fraction ξ is defined by Bilger et al.'s (1990) formula:

$$\xi = \frac{\frac{2(Z_{\mathrm{C}} - Z_{\mathrm{C,o}})}{W_{\mathrm{C}}} + \frac{Z_{\mathrm{H}} - Z_{\mathrm{H,o}}}{2W_{\mathrm{H}}} - \frac{Z_{\mathrm{O}} - Z_{\mathrm{O,o}}}{W_{\mathrm{O}}}}{\frac{2(Z_{\mathrm{C,f}} - Z_{\mathrm{C,o}})}{W_{\mathrm{C}}} + \frac{Z_{\mathrm{H,f}} - Z_{\mathrm{H,o}}}{2W_{\mathrm{H}}} - \frac{Z_{\mathrm{O,f}} - Z_{\mathrm{O,o}}}{W_{\mathrm{O}}}}. \qquad (16)$$

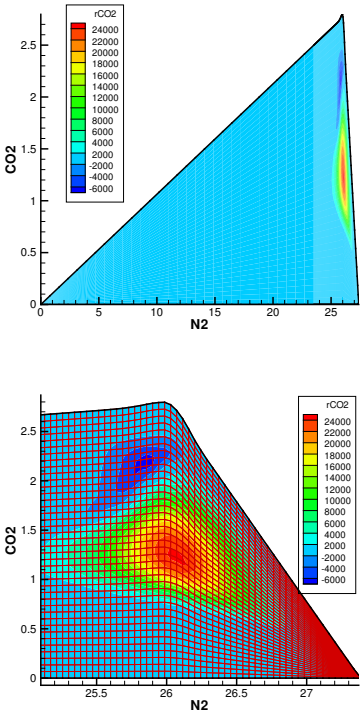

Figure 1: Rates of reaction progress (in mol/(kg s))) for the 2D-REDIM as a function of N_2 and CO_2 (specific mole numbers in units of kg/mol). Upper figure: entire tabulation domain; bottom: zoom of the domain around stoichiometry to visualize the mesh.

where Z_β is the total mass fraction of element β (conserved scalar) and W_β is the atomic mass of element β. The subscripts "f" and "o" refer to the fuel and oxidant streams.

In equations (4) and (5), $\boldsymbol{\phi} = (\xi, Y_{CO_2})$, and the chemical source term $S_{CO_2}(\boldsymbol{\phi})$ is given by the REDIM reduced chemistry.

Mixing model

As mixing model θ_α, the modified Curl's coalescence dispersion (CD) model is used, with $C_\phi = 2.0$. The CD micromixing model prescribes the evolution of particle composition as a series of pairwise mixing events. The particles participating in mixing are chosen at random from the set of particles present in a finite volume cell and their compositions change in the direction of the mixing partner. The degree of mixing in a pair is determined by a random variable, uniformly distributed between 0 (no mixing) and 1 (complete mixing) (Janicka et al., 1979; Wouters et al., 2002).

Implications for modelled equations for mean scalar, scalar variance and scalar flux

From Eq. (4) or (5), integration over the sample space yields the same mean scalar and scalar variance transport equations:

$$\frac{\partial\langle\rho\rangle\widetilde{\phi_\alpha}}{\partial t} + \frac{\partial\langle\rho\rangle\widetilde{U}_j\widetilde{\phi_\alpha}}{\partial x_j} = -\frac{\partial\langle\rho\rangle\widetilde{u''_j\phi''_\alpha}}{\partial x_j} + \langle\rho\rangle\widetilde{S_\alpha} + \underbrace{\langle\rho\theta_\alpha\rangle}_{=0}, \qquad (17)$$

$$\frac{\partial\langle\rho\rangle\widetilde{\phi''^2_\alpha}}{\partial t} + \frac{\partial\langle\rho\rangle\widetilde{U}_j\widetilde{\phi''^2_\alpha}}{\partial x_j} + 2\langle\rho\rangle\widetilde{u''_j\phi''_\alpha}\frac{\partial\widetilde{\phi_\alpha}}{\partial x_j} = -\frac{\partial\left\langle\rho u''_j\phi''^2_\alpha\right\rangle}{\partial x_j} - 2\langle\rho\rangle\widetilde{\phi''_\alpha S_\alpha} - 2\left\langle\rho\phi''_\alpha\theta_\alpha\right\rangle. \qquad (18)$$

There is no implicit summation over index α. The observation that the final term in Eq. (17) equals zero is a direct consequence of the mixing

model applied. In Eq. (18), the modelling of the scalar dissipation rate and molecular diffusion results from the mixing model θ_α. It is the same in both PDF approaches.

With the modelled joint scalar MDF, the gradient diffusion assumption, in accordance to the random walk model in the particle method, implies algebraic models for velocity-scalar correlations:

$$\langle \rho u_j'' \phi_\alpha'' \rangle = -\Gamma_T \frac{\partial \widetilde{\phi_\alpha}}{\partial x_j} \quad \text{and} \quad \langle \rho u_j'' \phi_\alpha''^2 \rangle = -\Gamma_T \frac{\partial \widetilde{\phi_\alpha''^2}}{\partial x_j}. \quad (19)$$

When the joint velocity-scalar MDF is considered, a differential scalar flux model is implied, depending on the Langevin model a_i and the mixing model θ_α. For instance, the modelled scalar flux transport equation takes the form:

$$\frac{\partial \langle\rho\rangle \widetilde{u_i'' \phi_\alpha''}}{\partial t} + \frac{\partial \langle\rho\rangle \widetilde{U}_j \widetilde{u_i'' \phi_\alpha''}}{\partial x_j} + \langle\rho\rangle \widetilde{u_j'' \phi_\alpha''} \frac{\partial \widetilde{U}_i}{\partial x_j} + \langle\rho\rangle \widetilde{u_i'' u_j''} \frac{\partial \widetilde{\phi}_\alpha}{\partial x_j}$$
$$= -\frac{\left\langle \rho u_j'' u_i'' \phi_\alpha'' \right\rangle}{\partial x_j} + \langle\rho\rangle \widetilde{u_i'' S_\alpha} + \left\langle \rho a_i \phi_\alpha'' \right\rangle + \left\langle \rho u_i'' \theta_\alpha \right\rangle. \quad (20)$$

Thus, there is a difference in modelling of the scalar flux and higher order velocity-scalar fluctuation correlations.

TEST CASE

The fuel (50% H_2 and 50% CH_4 by volume) is injected in the centre of the bluff-body burner through an injector of diameter $D_j =$ 3.6mm. The bluff body of diameter $D_b = 50$mm is surrounded by an unconfined coflowing air stream. Fuel and air are mixed in the recirculation zone behind the bluff body where chemical reaction can occur. The resulting hot products stabilise the flame.

In HM1 the jet and coflow bulk velocities were respectively 118m/s and 40m/s, while for HM3, the fuel jet velocity is $214 m/s$ (Dally and Masri, 1998; Dally et al., 1998). The numerical settings are similar to the calculations of flame HM1e presented by Naud et al. (2006). A $6D_b$-long and $3D_b$-wide 2D computational domain is used. Free-slip boundary conditions are prescribed on the bluff-body surface and on the lateral boundary. A convective outlet boundary condition, as presented by Sohankar et al. (1998), is used in order to avoid reflecting waves. Inlet boundary conditions are specified at cell centres in the same way as done by Muradoglu et al. (2003). Results are obtained on a 160×128 cartesian grid stretched both in axial and radial directions.

An average of 100 particles per cell is used. Iteration averages are made over 500 iterations. Converged results, obtained with an assumed-shape PDF method, are used as initial conditions. About 1000 outer iterations (5000 particle time steps) are enough to reach a stationary solution. Results obtained after 15000 particle time steps are now discussed.

RESULTS

Mean velocity and Reynolds stresses

The results for mean velocities and velocity fluctuations are very similar to the results of Naud et al. (2006) or Muradoglu et al. (2003) or Liu et al. (2005) for HM1 (not here shown due to space limitations). Good agreement with experimental data is found within the recirculation zone. The agreement deteriorates in the neck zone and the jet-like zone (from about $x = 1.8D_b$). Similar findings are observed for HM3. The downstream discrepancies have been observed in the different RANS calculations presented at the TNF workshops (http://www.ca.sandia.gov/TNF). An important observation for the present study is that the very small differences between scalar PDF and velocity-scalar PDF results (due to some differences in mean density) are negligible, even for flame HM3.

Mean composition

Figs. 2 and 3 show mean radial profiles for mean mixture fraction and temperature for flame HM1. Significant differences between

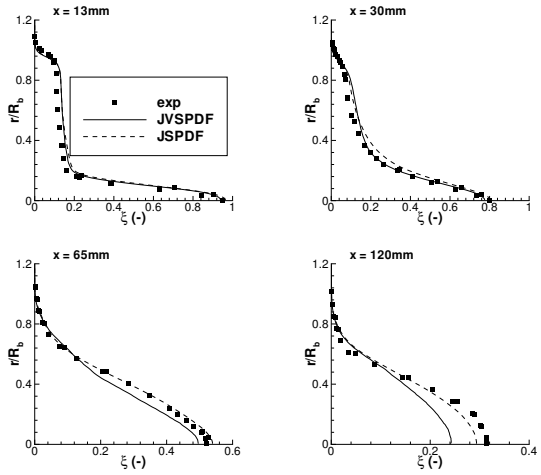

Figure 2: Radial profiles of mean mixture fraction (HM1).

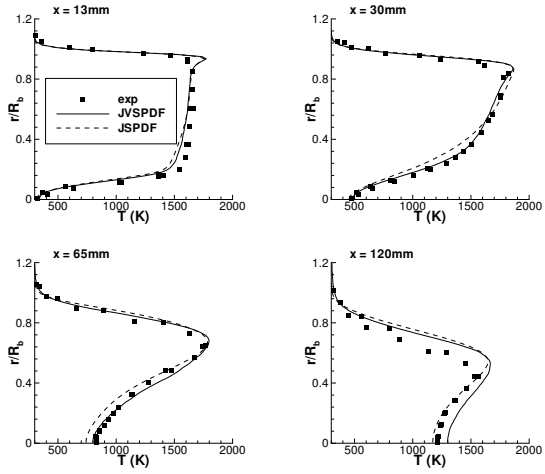

Figure 3: Radial profiles of mean temperature (HM1).

JSPDF and JVSPDF results are observed. Within the recirculation region, the quality of the JVSPDF results is better than the JSPDF results. In the neck zone, mean mixture fraction is in general underpredicted with the JVSPDF approach, though. As the convective terms in the modelled transport equations are very similar and the turbulence level is practically the same, too, the differences between JVSPDF and JSPDF must be due to differences in the scalar fluxes. This requires further investigation. We also note that the mean temperatures are in general somewhat lower in the JSPDF simulations. As the level of local extinction is comparable to the JVSPDF results (see scatter plots below), the mean temperature differences are due to differences in mean mixture fraction.

Figs. 4 and 5 show that the observations are very similar for the computational results of flame HM3. The temperatures obtained for HM3 are somewhat lower than for HM1, due to the occurrence of more local extinction (see below). There is no excellent agreement with experimental data, though. Note that Merci et al. (2006b) report that, in contrast to experimental observations, no stationary solution could be obtained for JSPDF results with the CD mixing model for flame HM3. In the present study, the limit cycle, reported in that reference, is not found, possibly due to the application of the REDIM chemistry model instead of a C_1 skeletal mechanism. Better agreement with experimental data can also most probably be obtained by applying more detailed chemistry mechanisms. This requires further investigation.

Mixture fraction variance

In Figs. 6 and 7, differences are observed for radial profiles of mixture fraction variance. In general, the JSPDF results are in better correspondence with the experimental data. The results are slightly

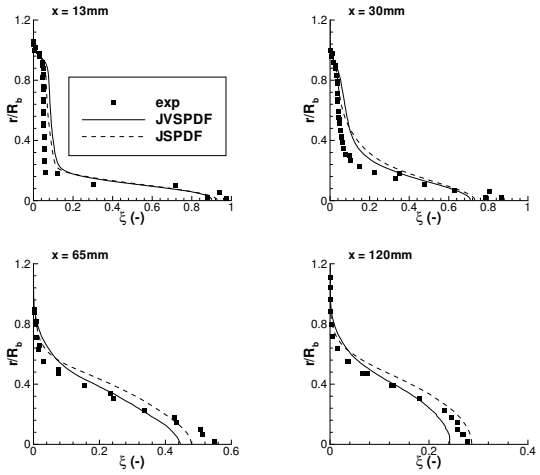

Figure 4: Radial profiles of mean mixture fraction (HM3).

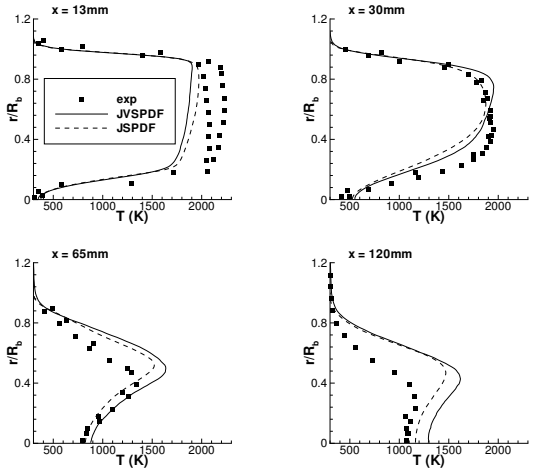

Figure 5: Radial profiles of mean temperature (HM3).

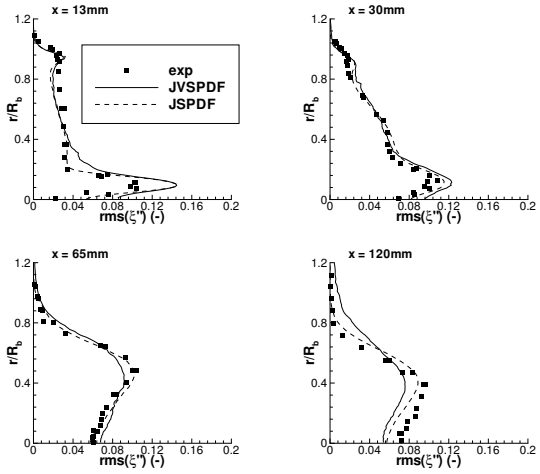

Figure 6: Radial profiles of mixture fraction variance (HM1).

better than reported by Merci et al. (2006b).

It is clear that the observed differences between JVSPDF and JSPDF are related to differences in mean mixture fraction, as well as to the modelling of velocity-scalar correlations: the scalar flux $u_j''\widetilde{\xi''}$ appearing in the production term and the triple correlation $u_j''\widetilde{\xi''\xi''}$ appearing in the turbulent diffusion term in Eq. (18).

Results in composition space: scatter plots

Figs. 8 and 9 reveal that, in composition space, differences between

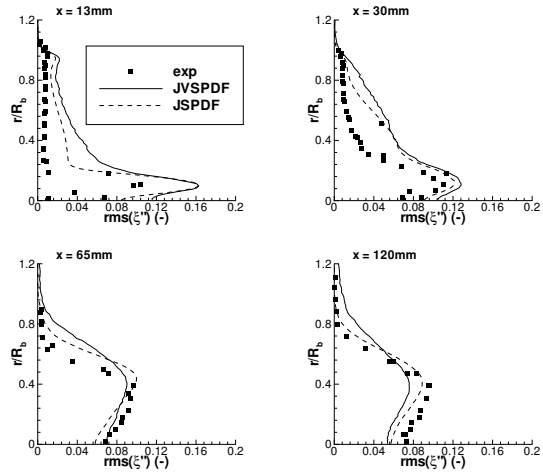

Figure 7: Radial profiles of mixture fraction variance (HM3).

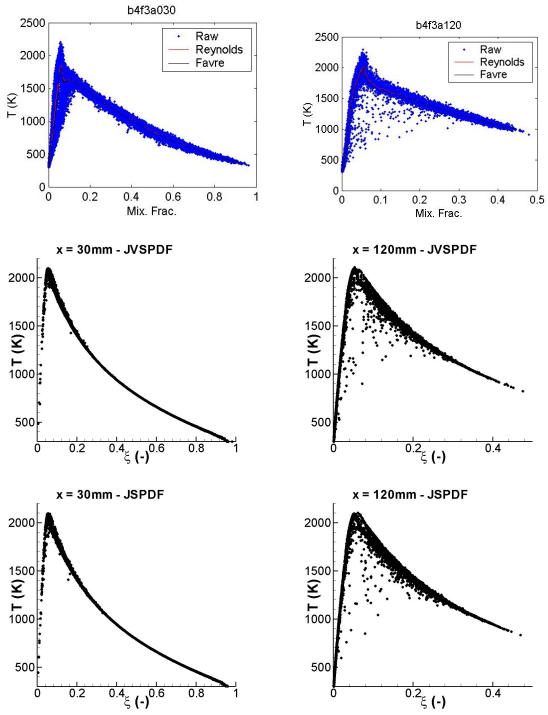

Figure 8: Scatter plots for temperature (HM1).

JSPDF and JVSPDF results are small, with the turbulence, chemistry and micro-mixing models applied. There is slightly more local extinction with JSPDF. The level of scatter in the present results, obtained with the CD mixing model, is in better correspondence with the experimental data than in the results of Liu et al. (2005), obtained with the EMST mixing model. This is the reason for using the CD mixing model in the present study.

CONCLUSIONS

A fair comparison of scalar PDF and velocity-scalar PDF modelling has been conducted for the bluff-body flames HM1 and HM3. Differences in the predicted turbulent flow fields are negligible. Significant differences are observed in results for mean mixture fraction and temperature and mixture fraction variance. These are attributed to implied modelling differences in the scalar fluxes (and higher order correlations). In general, joint velocity-scalar PDF results (implying a differential scalar flux model) are not better than joint scalar PDF results (based on gradient diffusion assumption), for the turbulence (LRR-IPM), chemistry (REDIM) and micro-mixing (CD) model applied. The impact of the choice JSPDF vs. JVSPDF on scatter plots is

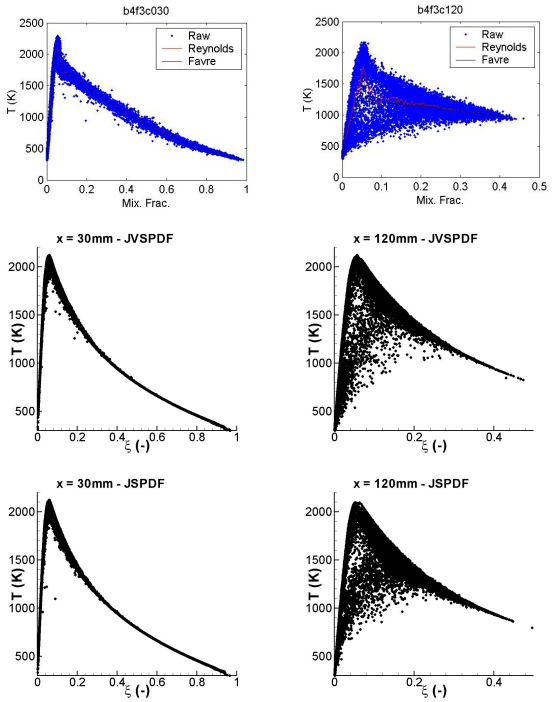

Figure 9: Scatter plots for temperature (HM3).

small for the test cases under study, with a slightly higher level of local extinction in the JSPDF results. The scatter plots are in good agreement with experimental data.

ACKNOWLEDGEMENTS

The first author is Postdoctoral Fellow of the Fund of Scientific Research – Flanders (Belgium) (FWO-Vlaanderen). This collaborative research is supported by the COMLIMANS program, by the Spanish MEC under Project ENE 2005-09190-C04-04/CON and by the Fund of Scientific Research – Flanders (Belgium) (FWO-Vlaanderen) through FWO-project G.0070.03.

REFERENCES

Bilger, R.W., Starner, S.H., and Kee, R.J., 1990, "On Reduced Mechanisms for Methane-Air Combustion in Nonpremixed Flames", Combustion and Flame, Vol. 80, pp. 135-149.

Bykov, V., and Maas, U., 2007, "The Extension of the ILDM Concept to Reaction-Diffusion Manifolds", Combustion Theory and Modeling, in press.

Cao, R.R., and Pope, S.B., 2005, "The Influence of Chemical Mechanisms on PDF Calculations of Nonpremixed Piloted Jet Flames", Combustion and Flame, Vol. 143, pp. 450-470.

Chevalier, C., and Warnatz, J., personal communication.

Dally, B.B., and Masri, A.R., 1998, "Flow and Mixing fields of Turbulent Bluff-Body Jets and Flames", Combustion Theory and Modelling, Vol. 2, pp. 193-219.

Dally, B.B., Masri, A.R., Barlow, R.S., and Fiechtner, G.J., 1998, "Instantaneous and Mean Compositional Structure of Bluff-Body Stabilized Nonpremixed Flames", Combustion and Flame, Vol. 114, pp. 119-148.

Janicka, J., Kolbe, W., and Kollmann, W., 1979, "Closure of the Transport Equation for the Probability Density Function of Turbulent Scalar Fields", Journal of Non-Equilibrium Thermodynamics, Vol. 4, pp. 47-66.

Jenny, P., Pope, S.B., Muradoglu, M., and Caughey, D.A., 2001, "A Hybrid Algorithm for the Joint PDF Equation of Turbulent Reactive Flows", Journal of Computational Physics, Vol. 166, pp. 218-252.

Launder, B.E., Reece, G.J., and Rodi, W., 1975, "Progress in the Development of a Reynolds-Stress Turbulence Closure", Journal of Fluid Mechanics, Vol. 68, pp. 537-566.

Li, G., Naud, B., and Roekaerts, D., 2003, "Numerical Investigation of a Bluff-Body Stabilised Nonpremixed Flame with Differential Reynolds-Stress Models", Flow, Turbulence and Combustion, Vol. 70, pp. 211-240.

Liu, K., Pope, S.B., and Caughey, D.A., 2005, "Calculations of Bluff-Body Stabilized Flames using a Joint Probability Density Function Model with Detailed Chemistry", Combustion and Flame, Vol. 141, pp. 89-117.

Merci, B., Roekaerts, D., and Naud, B., 2006a, "Study of the Performance of Three Micromixing Models in Transported Scalar PDF Simulations of a Piloted Jet Diffusion Flame ("Delft Flame III")", Combustion and Flame, Vol. 144, pp. 476-493.

Merci, B., Roekaerts, D., Naud, B., and Pope, S.B., 2006b, "Comparative Study of Micro-Mixing Models in Transported Scalar PDF Simulations of Turbulent Non-Premixed Bluff Body Flames", Combustion and Flame, Vol. 146, pp. 109-130.

Muradoglu, M., Liu, K., and Pope, S.B., 2003, "PDF Modeling of a Bluff-Body Stabilized Turbulent Flame", Combustion and Flame, Vol. 132, pp. 115-137.

Muradoglu, M., and Pope, S.B., 2002, "A Local Time-Stepping Algorithm for Solving the Probability Density Function Turbulence Model Equations", AIAA Journal, Vol. 40, pp. 1755-1763.

Muradoglu, M., Pope, S.B., and Caughey, D.A., 2001, "The Hybrid Method for the PDF Equations of Turbulent Reactive Flows: Consistency Conditions and Correction Algorithms", Journal of Computational Physics, Vol. 172, pp. 841-878.

Naud, B., Jiménez, C., and Roekaerts, D., 2006, "A Consistent Hybrid PDF Method: Implementation Details and Application to the Simulation of a Bluff-Body Stabilised Flame", Progress in Computational Fluid Dynamics, Vol. 6, pp. 146-157.

Pope, S.B., 1985, "PDF Methods for Turbulent Reactive Flows", Progress in Energy and Combustion Science, Vol. 11, pp. 119-192.

Pope, S.B., 1994, "On the Relationship between Stochastic Lagrangian Models of Turbulence and Second-Moment Closures", Physics of Fluids, Vol. 6, pp. 973-985.

Pope, S.B., 2000, "Turbulent Flows", Cambridge University Press.

Ren, Z, and Pope, S.B., 2004, "An Investigation of the Performance of Turbulent Mixing Models", Combustion and Flame, Vol. 136, pp. 208-216.

Sohankar, A., Norberg, C., and Davidson, L., 1998, "Low-Reynolds-Number Flow around a Square Cylinder at Incidence: Study of Blockage, Onset of Vortex Shedding and Outlet Boundary Condition", International Journal for Numerical Methods in Fluids, Vol. 26, pp. 39-56.

Wouters, H.A., Peeters, T.W.J., and Roekaerts, D., 1996, "On the Existence of a Generalized Langevin model Representation for Second-Moment Closures", Physics of Fluids, Vol. 8, pp. 1702-1704.

Wouters, H.A., Peeters, T.W.J., and Roekaerts, D., 2002, "Joint Velocity-Scalar PDF Methods", Chapter 2 in *Closure Strategies for Turbulent and Transitional Flows (Ed. B. Launder and N. Sandham)*, Cambridge University Press, pp 626-655.